Ocean Sci., 21, 2631–2642, 2025 https://doi.org/10.5194/os-21-2631-2025 © Author(s) 2025. This work is distributed under the Creative Commons Attribution 4.0 License.





Enhancement of near-inertial waves by cyclonic eddy in the northwestern South China Sea during spring 2022

Qi'an Chen^{1,2}, Hongzhou Xu¹, Dongxiao Wang^{3,4}, Bo Hong⁵, Chunlei Liu^{6,7}, Zheyang Zhang¹, Huichang Jiang¹, Wei Song³, Tong Long¹, Ling Wang^{1,2}, Sumin Liu¹, and Rongjie Chen^{1,2}

Correspondence: Hongzhou Xu (hzxu@idsse.ac.cn) and Bo Hong (bohong@scut.edu.cn)

Received: 21 January 2025 - Discussion started: 13 February 2025

Revised: 28 August 2025 - Accepted: 28 August 2025 - Published: 28 October 2025

Abstract. By analyzing datasets derived from four moorings during spring 2022, this study provides direct evidence that near-inertial waves (NIWs) can be largely enhanced by a passing cyclonic eddy (CE) in the northwestern South China Sea. Results show that the enhancement of NIWs mainly occurred at north side of the CE due to asymmetry of eddy structure. In vertical, the enhancement concentrated at above 200 m and reached peaks at around 100 m. Significant energy transfer rates between the CE and NIWs appeared at the same depth of the enhancement can reach a magnitude of 10^{-8} m² s⁻³ at the CE's edge. Under the impact of the CE, power of the first five NIWs modes was promoted significantly and dominated by the second and third modes. Overall, the CE transferred energy to NIWs before near-inertial kinetic energy reaching its peaks, while NIWs gave energy back to the CE after the peaks.

1 Introduction

Near-inertial waves (NIWs) are ubiquitous features throughout the global ocean with frequencies near the Coriolis frequency f (Garrett, 2001). As dominant modes of high-frequency variability in oceans, they contain half of the kinetic energy in internal wave fields (Alford, 2003; Alford et al., 2016; Ferrari and Wunsch, 2009). NIWs transfer energy

from mixed layer to interior and ultimately dissipate into microscale turbulence, providing an energy source for abyssal diapycnal mixing (Chen et al., 2017; Ferrari and Wunsch, 2009). Therefore, NIWs are of vital importance for energy cascade among multiscale dynamic processes.

Due to horizontal spatial scales of 10–100 km and slow group speed of NIWs, they are likely to interact strongly with mesoscale eddies in oceans (Alford et al., 2016). Besides resonant frequency shifting from local f to the effective inertial frequency caused by mesoscale vorticity (Klein et al., 2003; Kunze, 1985; Weller, 1982), energy exchange between eddies and NIWs also plays an important role in oceanic energy cascade (Ferrari and Wunsch, 2009; Thomas, 2017). Researchers have stated that the NIWs can extract energy from eddy and affect the vertical material transport (Barkan et al., 2021; Esposito et al., 2023). Moreover, energy transfer from mean flows can balance the dissipation of near-inertial energy near the critical layer, thereby conserving near-inertial energy during eddy migration (Xu et al., 2022b).

Jing et al. (2017, 2018) suggested that there is a permanent energy transfer from eddies to NIWs under a positive Okubo–Weiss parameter condition. Furthermore, Yu et al. (2022) revealed that enhanced near-inertial kinetic energy (NIKE) is found preferentially in regions of anticyclonic vorticity. Using surface drifter dataset, Liu et al. (2023) indicated that bidirectional energy transfer exists between eddy

¹Institute of Deep-sea Science and Engineering, Chinese Academy of Sciences, Sanya, 572000, China

²University of Chinese Academy of Sciences, Beijing, 100049, China

³School of Marine Sciences, Sun Yat-sen University, Zhuhai, 519000, China

⁴South Marine Science and Engineering Guangdong Laboratory (Zhuhai), Zhuhai, 519082, China

⁵School of Civil and Transportation Engineering, South China University of Technology, Guangzhou, 510641, China

⁶College of Ocean and Meteorology, Guangdong Ocean University, Zhanjiang, 524088, China

⁷South China Sea Institute of Marine Meteorology, Guangdong Ocean University, 529568, Zhanjiang, China

and NIWs in the global oceans. Above studies all emphasized role of eddy on affecting frequencies of NIWs, NIKE as well.

As the largest semi-enclosed marginal sea in the northwestern Pacific Ocean, the South China Sea (SCS) has frequent eddy activities (Chen et al., 2011; Chu et al., 2014; Nan et al., 2011; Wang et al., 2003, 2008). Early studies, by using various eddy detection algorithms, have statistically characterized the mean properties of eddies, identifying peak occurrences along western boundary currents and shelf break regions (Lin et al., 2007; Wang et al., 2003; Xiu et al., 2010). Specifically, Chen et al. (2011) indicated that eddies occur 35 %-60 % of the time in the northern SCS, underscoring their critical role in regional oceanography. Recent advancements in remote sensing and in-situ observational technologies have enabled significant insights into eddy formation and their three-dimensional structures (Chu et al., 2022; He et al., 2018; Nan et al., 2011; Wang et al., 2023; Zhang et al., 2016). Due to their unique three-dimensional structures and spatiotemporal scales, eddies mediate significant material transport (He et al., 2018; Zhang et al., 2015, 2019) and substantial energy exchanges with internal waves and western boundary currents (Chu et al., 2014; Fan et al., 2024; Huang et al., 2018; Liu et al., 2023; Xu et al., 2022a; Zhang et al., 2023; Zhao et al., 2023).

In the northwestern SCS, large portion of eddies propagate westward and terminate near Xisha Trough (Fig. 1a) (Wang et al., 2003; Zhai et al., 2010), making this place as an ideal area for investigating NIWs and its interaction with eddies. However, interaction and energy exchange processes between them remain to be investigated in this area. In this study, four moorings, each equipped with a Teledyne RD Acoustic Doppler Current Profiler (ADCP), were deployed in the Xisha Trough of the northwestern SCS (Fig. 1a). During spring 2022, a cyclonic eddy (CE) propagated westward across the mooring array, giving an opportunity to study energy transfer between NIWs and the CE in this area. We introduce data and methods in Sect. 2, present the observation results in Sect. 3, discuss energy transfer between NIWs and the CE in Sect. 4, and give a conclusion in Sect. 5.

2 Methodology

2.1 Data

The four moorings (Q_1-Q_4) were deployed in the study area on 21–23 August 2021. One upward-looking 75 kHz ADCP along with a CTD (SBE 37sm) was fixed at approximately 480 m depth and continuously monitored current velocity for each mooring (Fig. 1b). The ADCPs were set to have 30 bins with 16 m of vertical interval and 30 min of temporal interval, enabling extraction of NIWs of the upper ocean. The moorings were recovered on 13–15 November 2022. Several ADCP bins near the sea surface were omitted due to large

fluctuations, and the remaining were vertically linearly interpolated to 1 m resolution. Due to the significant vertical fluctuations based on CTD data in certain periods, flow velocity compensation correction was applied to ADCP data, which was calculated based on depth change and flow direction.

The Copernicus Marine Environment Monitoring Service (CMEMS) provides daily geostrophic current and sea level anomaly (SLA) data with a resolution of $0.25^{\circ} \times 0.25^{\circ}$, which were used to detect eddy during the observation period. The $1/12^{\circ}$ three-dimensional products were obtained from CMEMS to calculate energy transfer rate between eddy and NIWs. The eddy dataset from Archiving, Validation, and Interpretation of Satellite Oceanographic (AVISO) was used to provide the trajectories and edges of the eddy. World Ocean Atlas (WOA18) data was used to extract temperature and salinity data. The European Centre for Medium-Range Weather Forecasts (ECMWF) Reanalysis V5 (ERA-5) data, which has hourly temporal and 0.25° spatial resolutions, was used to calculate near-inertial energy input from the wind field.

2.2 Method

The method for ADCP velocity flow velocity compensation correction is as follows:

$$V_{\text{true}}(t) = V_{\text{measured}}(t) + V_{\text{platform}}(t),$$
 (1)

$$V_{\text{platform}}(t) = \frac{\Delta x}{\Delta t} \mathbf{i} + \frac{\Delta y}{\Delta t} \mathbf{j}, \qquad (2)$$

$$(x, y) = (\rho \cos \theta \rho \sin \theta) \tag{3}$$

$$(\rho, \theta) = (\sqrt{L^2 - z_{\text{top}}^2}, \alpha), \tag{4}$$

where $V_{\rm true}$, $V_{\rm measured}$ and $V_{\rm platform}$ are the true velocity, observed velocity and the platform movement velocity, respectively. (ρ, θ) is the polar coordinate position of the ADCP with the initial position as the origin. L, $z_{\rm top}$ and α are the length of the rope at the position of the ADCP, the depth of the ADCP and the direction angle of the horizontal projection.

The eddy-NIW energy transfer rate ε , where a positive value indicates energy transfer from eddies to NIWs and a negative value denotes the reverse, can be quantitatively calculated following Jing et al. (2018):

$$\varepsilon = -\left(\langle \boldsymbol{u}_{i}\boldsymbol{u}_{i}\rangle - \langle \boldsymbol{v}_{i}\boldsymbol{v}_{i}\rangle\right)\frac{S_{n}}{2} - \langle \boldsymbol{u}_{i}\boldsymbol{v}_{i}\rangle S_{s},\tag{5}$$

where $S_{\rm n}=\frac{\partial u_{\rm g}}{\partial x}-\frac{\partial v_{\rm g}}{\partial y}$ and $S_{\rm s}=\frac{\partial u_{\rm g}}{\partial y}+\frac{\partial v_{\rm g}}{\partial x}$ are the normal strain and shear strain of the geostrophic velocity $u_{\rm g}$ and $v_{\rm g}$, which are obtained from the CMEMS three-dimensional reanalysis data (Chen et al., 2023). We used fourth-order Butterworth band-pass filter with the cutoff frequency (0.8 f–1.2 f) to separate near-inertial velocity $u_{\rm i}$ and $v_{\rm i}$ from the ADCP data. The $\langle \cdot \rangle$ represents a moving average of 3 internal wave periods.

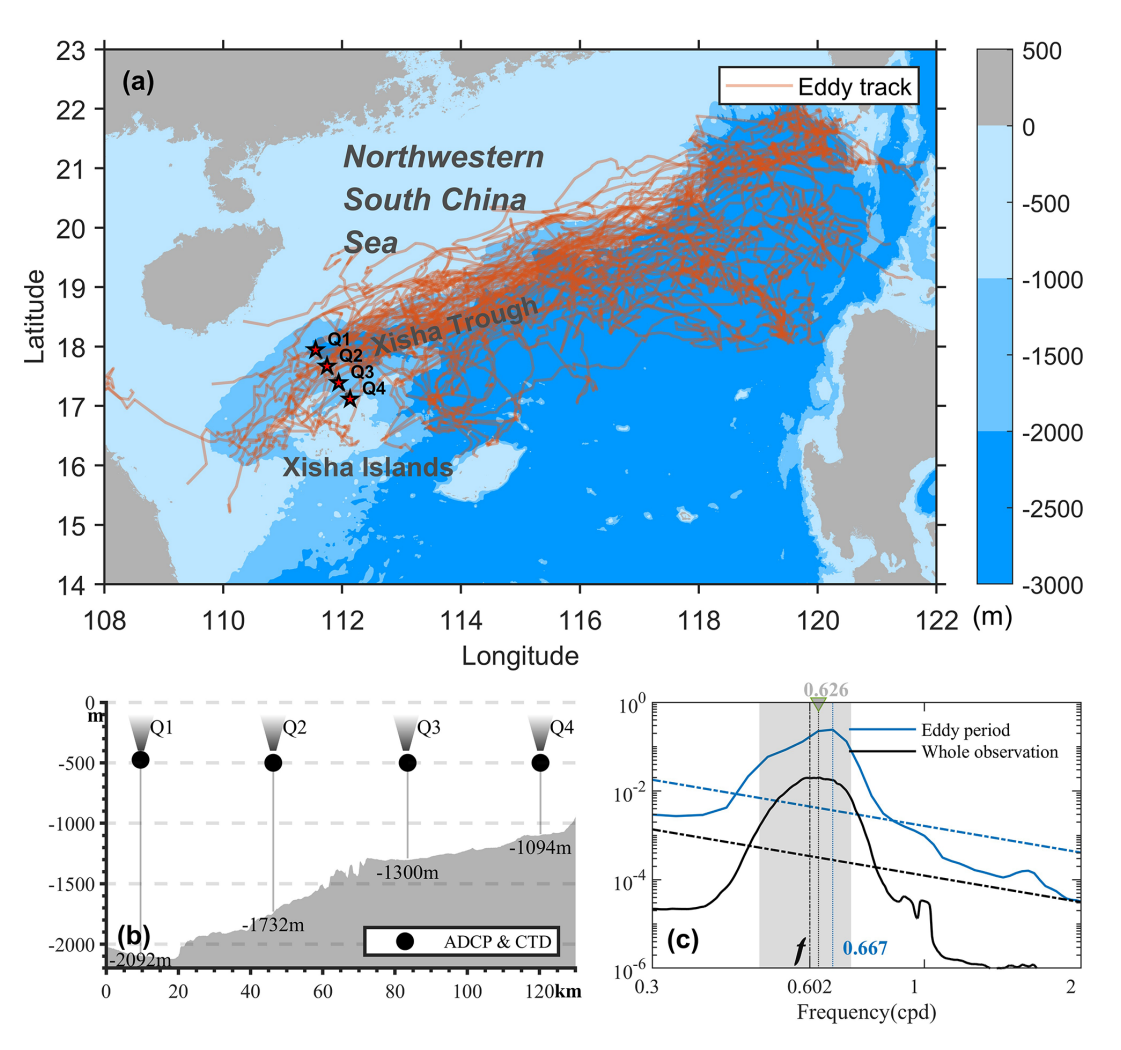


Figure 1. (a) Location of four moorings (Q_1-Q_4) in the northwestern SCS. The shaded background color represents topography. Orange lines indicate tracks of long-lasting eddy propagating from the Luzon area to the Xisha Trough from 1993 to 2023. **(b)** Structure of upward-looking ADCP mooring along the slope of topography. **(c)** The power spectra during eddy period (blue line) and whole observation period (black line). The spectra are averaged above 200 m.

Near-inertial wind work was estimated as (Alford, 2001; Dasaro, 1985; Voet et al., 2024):

$$W = \tau_{\mathbf{i}} \cdot u_{\mathbf{i}},\tag{6}$$

where u_i is near-inertial velocity at sea surface derived from CMEMS products and τ_i is bandpassed near-inertial wind stress after calculated as (Alford, 2020; Liu et al., 2019):

$$\tau = \rho_{\rm a} C_{\rm D} | U_{10} - u_{\rm c} | (U_{10} - u_{\rm c}), \tag{7}$$

where $\rho_a = 1.3 \,\mathrm{kg} \,\mathrm{m}^{-3}$ is density of air, U_{10} is 10 m wind velocity vector derived from ERA5 data, $u_{\rm c}$ is ocean current vector derived from CMEMS data, $C_{\rm D}$ is drag coefficient (Oey et al., 2006).

We used the Okubo-Weiss parameter (OW) (Provenzale, 1999) method to detect the CE. The OW parameter was computed from the horizontal velocity field as follows:

$$\sigma = S_{\rm sh}^2 + S_{\rm st}^2 - \zeta^2,\tag{8}$$

where $S_{\rm sh} = \frac{\partial u}{\partial y} + \frac{\partial v}{\partial x}$ and $S_{\rm st} = \frac{\partial u}{\partial x} - \frac{\partial v}{\partial y}$ are the shear and strain deformation, respectively, and ζ is the relative vorticity.

3 Results

3.1 Near-inertial frequency and NIKE

The snapshots of SLA and surface geostrophic velocity fields show that the CE approached the mooring array on 1 February (Fig. 2). Its center passed through Q_3 around 26 February and it left the mooring array on 9 March. During the entire observation period, NIWs exhibited a small blue shift of near-inertial frequency with a peak value of 0.616 cpd (cycles per day) (Fig. 1c), while a significant blue shift occurred during the eddy period (1 February–9 March) due to the background positive vorticity of the CE. The peak of

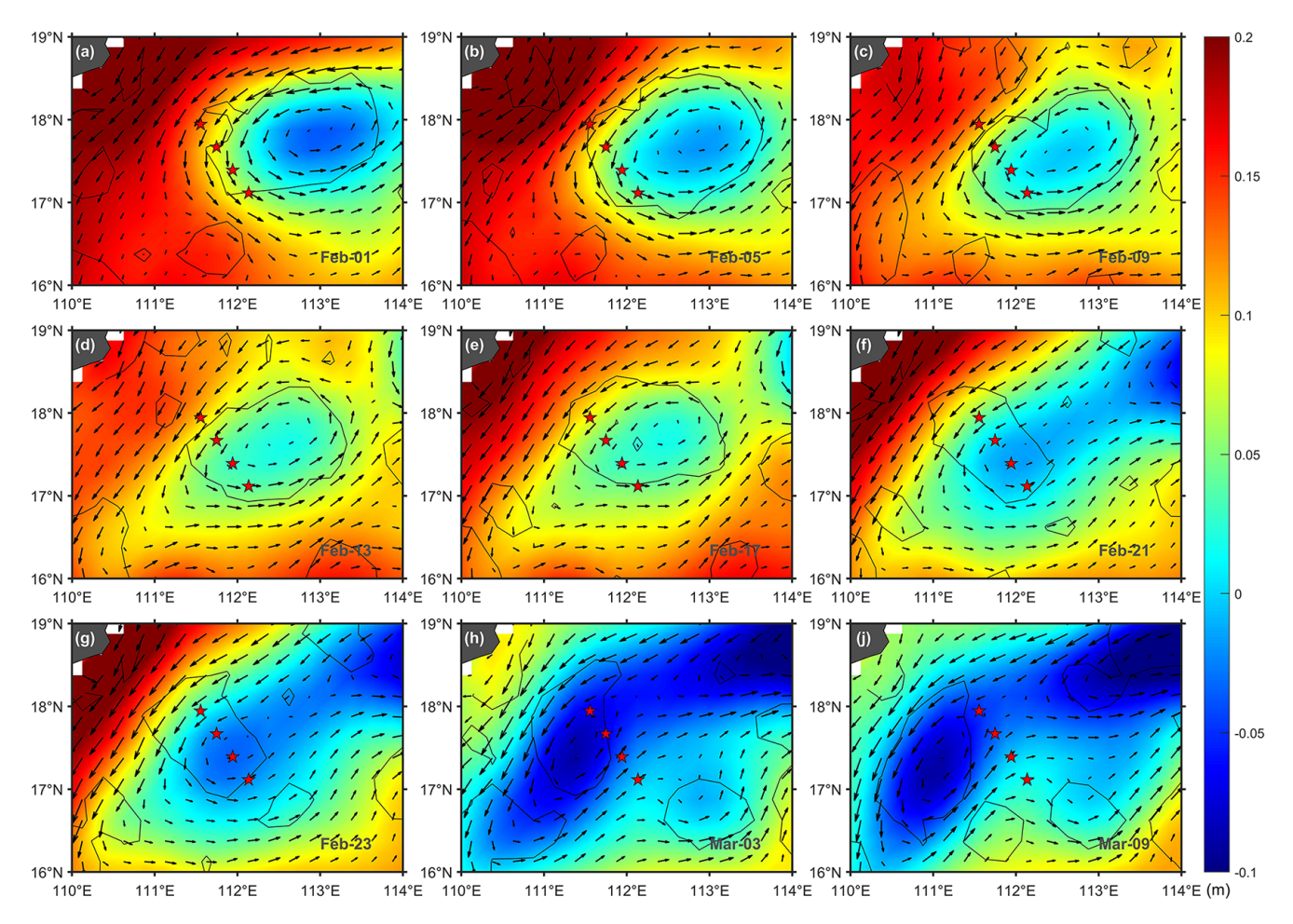


Figure 2. (a-j) The snapshot of sea level anomaly and geostrophic current vector during 1 February–9 March. The black line indicates the Okubo–Weiss parameters.

spectral frequency ($\omega_{\rm p}$) reached 0.667 cpd, with a relative frequency shift ($\frac{\omega_{\rm p}-f}{f}$, RFS) of about 10.8% in this area. It is significantly larger than the global RFS (Guo et al., 2021), suggesting significant impact of the CE on local nearinertial frequencies. The observed near-inertial spectral peak, $\omega_{\rm p}=0.667$ cpd, in the CE is consistent with the effective inertial frequency, $f_{\rm eff}=f+\zeta\approx0.69$ cpd, estimated from surface geostrophic currents and the local inertial frequency.

Horizontal velocity wavelet power spectra show that strong power of NIWs occurred during eddy period but with large variations at different eddy stages (Fig. 3a–d). To quantify NIKE at different stages of the CE, we defined two time periods named as Period 1 (16–26 February) and Period 2 (26 February–8 March), covering 10 d before and after the eddy's center passed through the mooring array. In addition, no eddy period with calm wind during 1–20 June was chosen for extra comparison. Figure 3e–h shows temporal and vertical variations of NIKE at the four moorings during eddy period. The missing data of NIKE at surface layers are due to mooring swing caused by strong currents. It can be seen

that NIKE was enhanced largely at above 200 m during Period 2. And peak values of NIKE concentrated at around 100 m. The time-averaged NIKE during Period 2 has almost an order of magnitude larger than that during the no eddy period (Fig. 3i–l), suggesting significant impact of the CE on local NIKE. Moreover, NIKE illustrates asymmetry in space during eddy period (Fig. 3e–l). At north side of the CE (Q_1 – Q_2), NIKEs became much stronger than that at south side of the CE (Q_3 and Q_4), especially at Q_2 with a maximum value up to 12.0 J m⁻³ (Fig. 3f), which has the same magnitude as the result observed by Xu et al. (2022b).

3.2 Impact of eddy on NIWs

To ensure the fact that the CE could largely enhance NIWs in the northwestern SCS, we compared time series of vertical-integrated (above 200 m) NIKE at each mooring with mooring-eddy distance, wind-input NIKE and eddy kinetic energy (EKE) in the study area (Figs. 4 and 5). NIWs were enhanced gradually accompanied by weakening EKE during Period 1 when wind-input NIKE was relatively stable

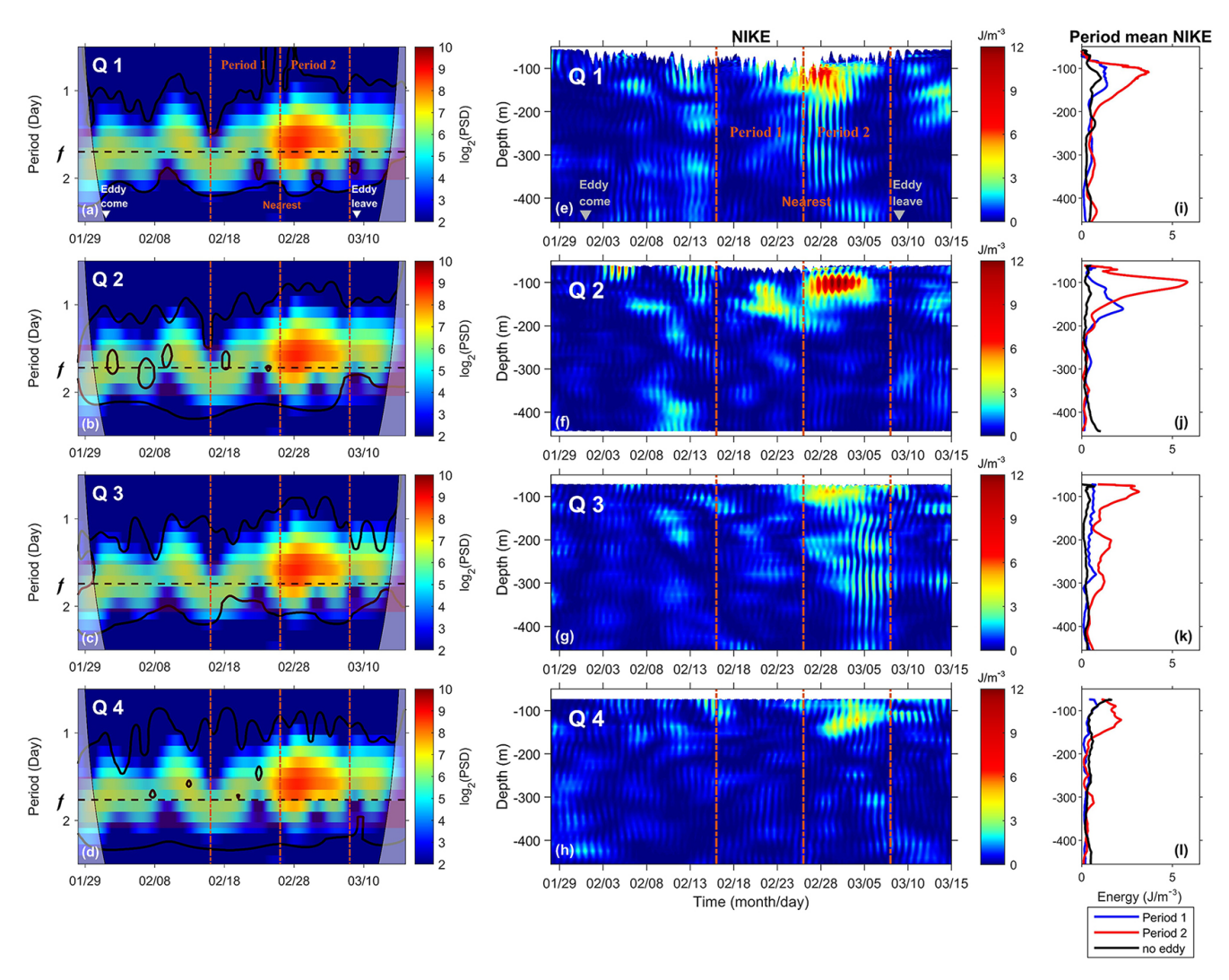


Figure 3. (a–d) 100 m-depth horizontal velocity wavelet power spectra at Q_1 – Q_4 during eddy period. (e–h) Vertical distribution of NIKE at Q_1 – Q_4 . The gray triangles indicate the time when the CE edge contacts and leaves the mooring array. (i–l) Vertical distribution of time-averaged NIKE during "no eddy period" (black line), "Period 1" (blue line), and "Period 2" (red line) at Q_1 – Q_4 . The red dashed lines mark two periods of the CE.

and minor. The wind work during the eddy period is about several orders of magnitude smaller than that affected by typhoons (Ouyang et al., 2022; Yuan et al., 2024) and several times smaller than the wind work results of Voet et al. (2024) in the Iceland basin. Results suggest a vivid energy transfer from Eddy to NIWs during this period that will be quantified and discussed in Sect. 4. After passing of the CE's center, the CE enhanced NIWs faster, indicating more energy transfer from eddy to NIWs during Period 2 than that during Period 1. The slight increase of EKE during Period 2 was contributed by background western boundary current velocity input (Fig. 2).

In space, NIWs intensity reached $600 \,\mathrm{J}\,\mathrm{m}^{-2}$ at Q_2 , whereas values at Q_3 and Q_4 were approximately $300 \,\mathrm{J}\,\mathrm{m}^{-2}$. This difference may be associated with the CE's vorticity dis-

tribution, where relative vorticities observed north of the CE (between Q_1 – Q_2) were notably stronger than those measured south of the CE (between Q_3 – Q_4) (Fig. 6). Zhao et al. (2021, 2023) pointed out that NIWs generation is significantly influenced by the eddy structure in which eddy with stronger shears tend to generate more powerful NIWs. In our case, Fig. 2 shows that the north side of the CE exhibited spatial overlap with the western boundary current of the northwestern SCS (Fig. 2) where strong shear could enhance NIWs largely at this side (Zhao et al., 2021, 2023).

3.3 Impact of eddy on near-inertial modes

The CE not only affected frequency and energy of NIWs, but also their modes in the study area. Here, we calculated vertical-averaged energy (above 200 m) of the first five

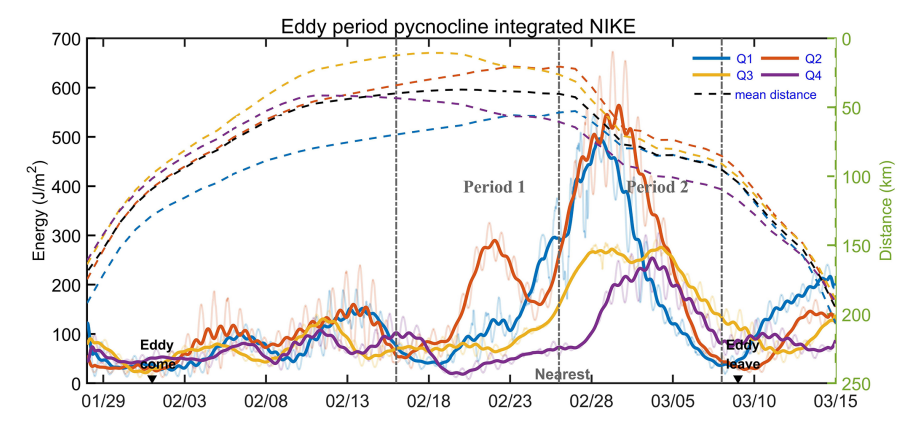


Figure 4. Time series of raw (thin lines) and daily-smoothed (thick lines) depth-integrated (above 200 m) NIKE at Q_1 – Q_4 (solid lines) accompanying with distance between the CE's center and each mooring (dashed lines) during eddy period. The black dashed line represents the mean distance between the CE's center and four moorings. The triangles mark the time when the eddy edge contacts and leaves the mooring array.

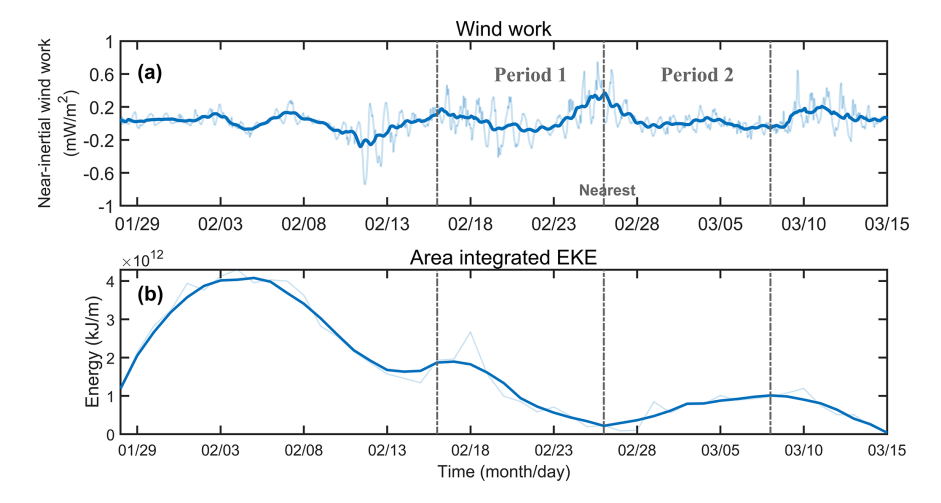


Figure 5. (a) Time series of raw (thin lines) and daily-smoothed (thick lines) averaged wind-input NIKE at Q_1-Q_4 . (b) Time series of raw (thin lines) and daily-smoothed (thick lines) area integrated EKE.

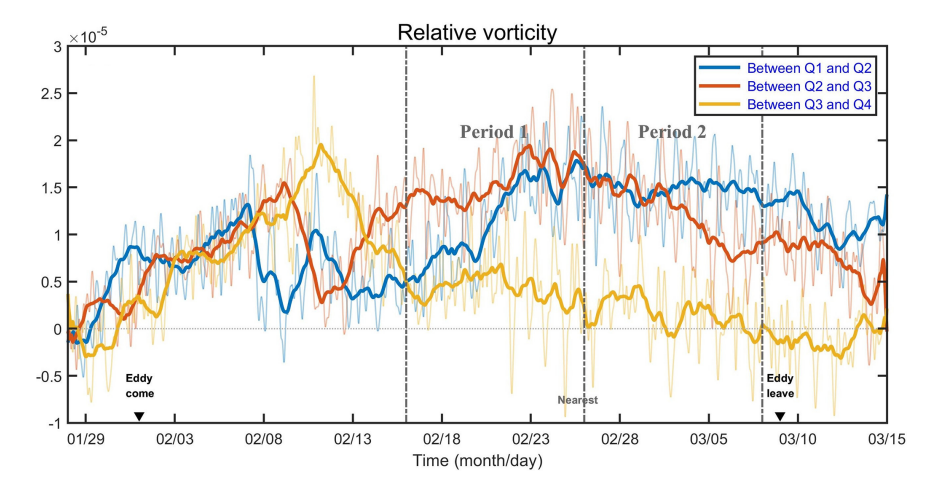


Figure 6. Time series of raw (thin lines) and daily-smoothed (thick lines) relative vorticity among four moorings. Vertical gray dashed lines mark two periods of the CE.

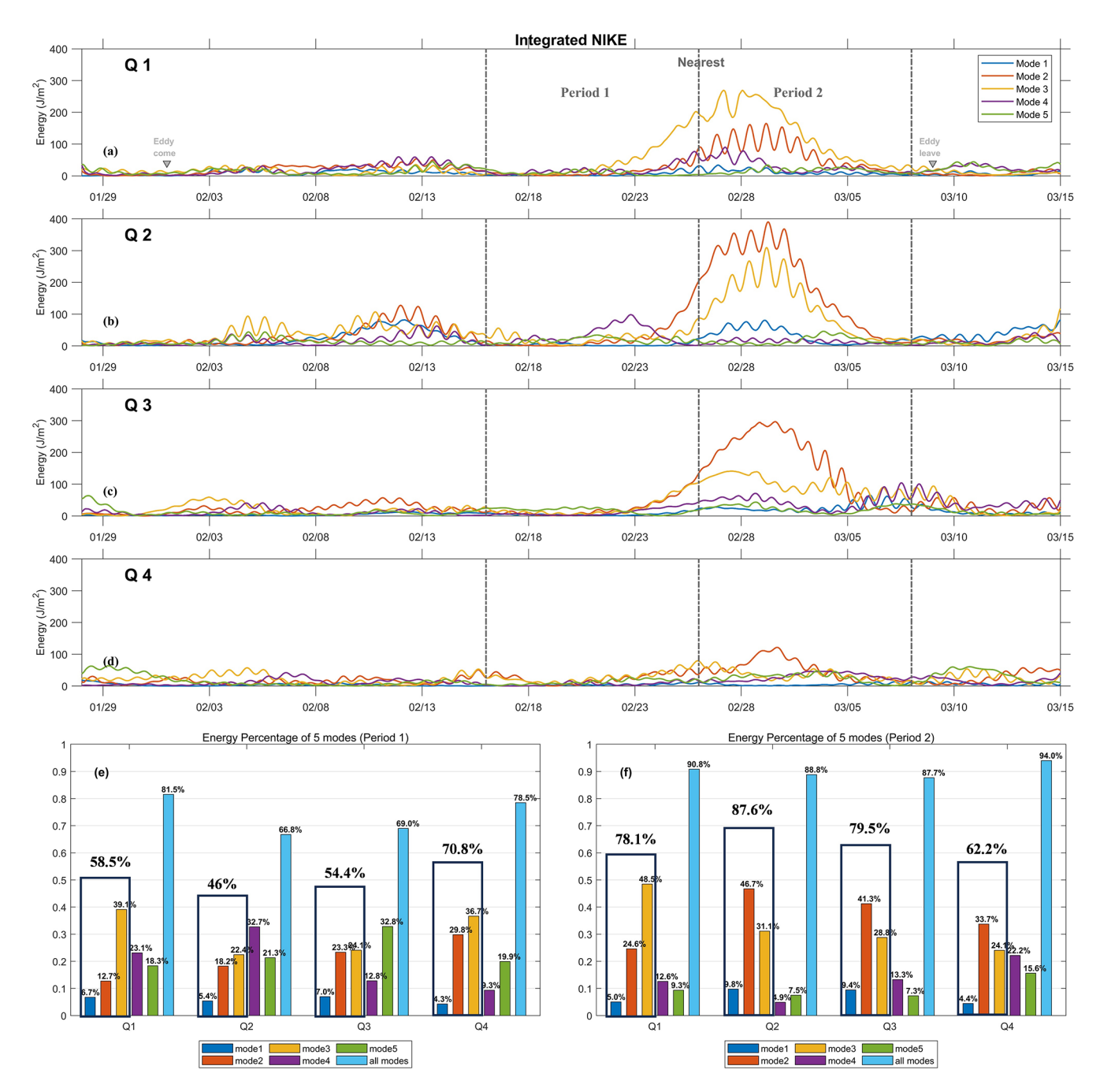


Figure 7. (a-d) Time series of NIKE for the first five modes at Q_1-Q_4 during eddy period. (e, f) The time-averaged proportions of each mode and all five modes during period 1 and period 2 at Q_1-Q_4 . Black border indicates proportion sum of the first three modes.

modes of near-inertial velocity during eddy period (Fig. 7a–d). All five modes grew since Period 1 and reached peak values at Period 2. But the CE had different influence on different modes with low modes (mainly the second and third modes) being significantly enhanced, especially near the CE's center. Low modes rose from 46 % (Q_2) and 54.4 % (Q_3) of total energy during Period 1 to 87.6 % (Q_2) and 79.5 % (Q_3) during Period 2, respectively (Fig. 7e and f). The first mode has longer vertical wavelength and propagates

faster than other modes that make it easy escape from eddy's influence (Chen et al., 2013). Overall, energy proportion of the first five modes were promoted from 81.5%, 66.8%, 69%, and 78.5% during Period 1 to 90.8%, 88.8%, 87.7%, 94% at Q_1-Q_4 , respectively (Fig. 7e and f). In conclusion, the cyclonic eddy has a prominent influence on different modes of NIWs, resulting in the intensification of lower-mode energy within its core region, especially for modes 2 and 3.

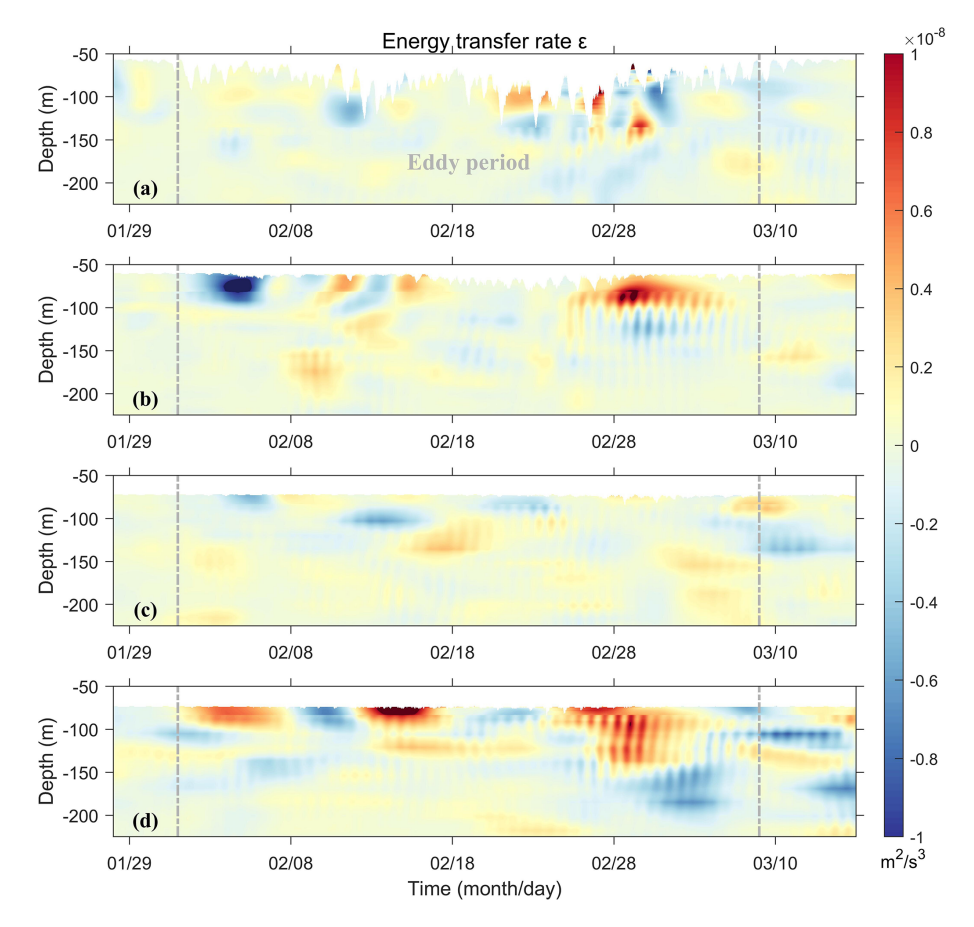


Figure 8. (a-d) Vertical distribution of energy transfer rate between the CE and NIWs at Q_1-Q_4 during eddy period.

4 Discussion

Energy exchange between eddies and NIWs is one of the most important processes in oceanic energy cascade (Alford et al., 2016; Ferrari and Wunsch, 2009; Thomas, 2017). By simulations, Jing et al. (2017) found that the energy transfer efficiency from eddies to NIWs is about 2% of the near-inertial energy input by the wind in the Kuroshio Extension region. Based on surface drifter dataset, Liu et al. (2023) stated that energy transfer efficiency can reach about 13 %, indicating previous underestimation of eddy impact on NIWs. For obtaining precise results, direct ocean current measurement by long-term mooring is essential (Jing et al., 2018). In this section, eddy-NIWs energy transfer rate during eddy period in the study area is quantified and discussed (Fig. 8). Corresponding to the layer of NIKE enhancement (Fig. 3), large energy transfer rates occurred at above 200 m with the peak values at around 100 m during eddy period, rather than surface and mixing layers (Jing et al., 2017; Liu et al., 2023). Both positive and negative transfer rates can reach a magnitude of 10^{-8} m² s⁻³ in the study area, in which they are of same order of magnitude as the results reported by Chen et al. (2023) in the Northwestern

Pacific Ocean, but they are significantly stronger than the results of Jing et al. (2018) in the Gulf of Mexico. The differences may be attributed to the strength of eddies, their rotation direction and the intensity of NIWs. Previous studies have shown that eddy rotation plays a critical role in energy transfer and NIWs propagation due to differences in vorticity input and stratification modulation (Alford et al., 2016; Jing et al., 2017). In addition, eddy-NIWs energy transfer is largely dependent on eddy structure in which high rate can be caused by strong eddy shear (Zhao et al., 2023). It can be found that energy transfer at Q_1 , Q_2 and Q_4 were more active than that at Q_3 due to occurrence of large shear strain at CE's edge (Fig. 9a and b). Although NIKEs at Q_4 were relative weak, the strong shear strains of the low frequency flow promoted local transfer rates at this area. Thomas and Daniel (2020) and Li et al. (2022) both stated that NIWs draw energy from the background flow when the energy of NIWs is small compared to that of the background flow, and release energy to the background flow when the energy of NIWs is large compared to that of the background flow. Similarly, our results show that positive/negative energy transfers from the CE to NIWs dominated "Before Strongest"/"After Strongest" periods at most mooring stations (Fig. 9c), in-

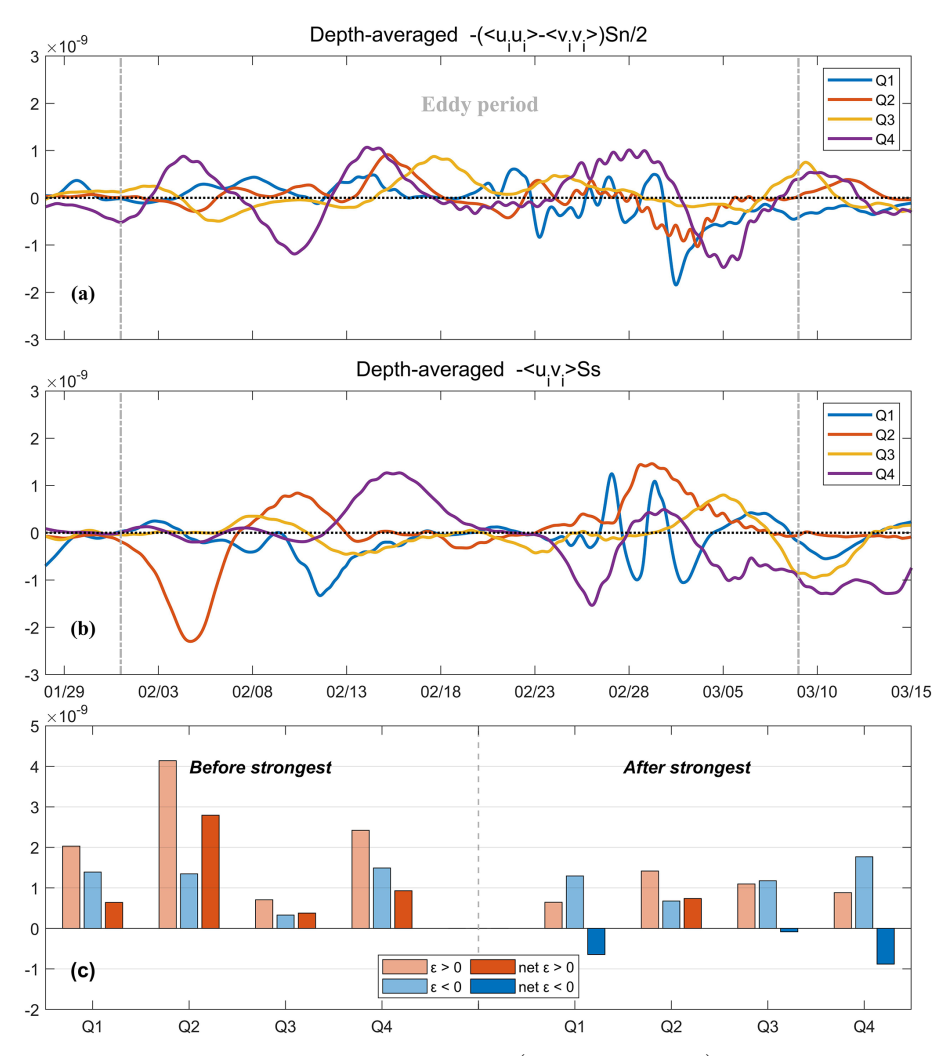


Figure 9. (a) Time series of depth-averaged (above 200 m) normal strain $\left(-\langle u_i u_i \rangle \langle v_i v_i \rangle\right) \frac{S_n}{2}\right)$ of the CE for each mooring. (b) Time-series of depth-averaged (above 200 m) shear strain $\left(-\langle u_i v_i \rangle S_s\right)$ of the CE for each mooring. (c) Time- (7 d) and depth-averaged (above 200 m) positive (light red), negative (light blue) and net transfer rate (dark red and blue indicate positive and negative values) before and after the NIKE reaching its peak at $Q_1 - Q_4$.

dicating an inhomogeneous and bidirectional energy transfer between eddy and NIWs during different periods in the northwestern SCS. Moreover, we compared the energy transferring from the CE to the NIWs with net NIKE increasement during "Before Strongest" period. Here, we multiplied the net energy transfer rate by density, then integrated them over the 0–200 m depths during "Before strongest" period as:

 $T_{\rm strongest}$ 0 m $\int_{T_{\rm strongest}-7\,{\rm days}} \int_{-200\,{\rm m}} \rho_0 \overline{\varepsilon} {\rm d}z {\rm d}t$, in which $\overline{\varepsilon}$ represents net en-

 $T_{\rm strongest}$ –7 days –200 m ergy transfer rate. Results show that there were 79, 346, 47, and 115 J m⁻² energy transferring from the CE to the NIWs during the period at Q_1 – Q_4 , respectively, which account for about 16 %, 88 %, 27 %, and 47 % of the net NIKE increasements (492, 394, 175 and 245 J m⁻² at Q_1 – Q_4 , respectively) . In average, they account for approximately 45 % of the net

NIKE increasement (325 J m⁻²) in this area indicating a key role of mesoscale eddy on NIWs in the Northwestern SCS.

5 Conclusion

During spring 2022, the CE passed through the northwestern SCS. Our four long-term moorings with ADCP instruments captured the interaction and energy exchange processes between eddy and local NIWs for the first time in this area. We found that NIWs can be largely enhanced by the passing CE. Horizontally, the CE transferred more energy to NIWs at the north side than that at the south side of the CE. This disparity may be attributed to the eddy asymmetry with stronger relative vorticity and shear in the northern region, which can significantly amplify NIWs generation (Zhao et al., 2021, 2023). In vertical, the enhancement of NIKE occurred at

above 200 m, with a maximum exceeding 12 J m⁻³ at a depth of 100 m. Power comparison of different NIWs modes during eddy period indicate that the CE promoted percentage of first five modes, especially the second and third modes. Overall, NIWs drew energy from the CE during the enhancing period of NIKE, while they gave energy back to the CE during weakening period of NIKE. This study is helpful for understanding multi-scale interaction and energy cascade in the northwestern SCS.

Data availability. The CMEMS products are available at https: //data.marine.copernicus.eu/product/GLOBAL_MULTIYEAR_ PHY_001_030/services (last access: 18 March 2024). The ERA-5 wind data are available at https://doi.org/10.24381/cds.adbb2d47 (Hersbach et al., 2023). The WOA2018 climatological monthly mean mixed layer depth data are available at https://www.ncei.noaa.gov/access/world-ocean-atlas-2018/ access: 26 April 2020). The AVISO eddy data are available at https: //www.aviso.altimetry.fr/en/data/products/value-added-products/ global-mesoscale-eddy-trajectory-product.html (last 24 December 2024). The bathymetric data is from GEBCO Gridded Bathymetry Data (https://download.gebco.net, last access: 28 June 2022). The data used for plotting figures for this paper are available at https://doi.org/10.5281/zenodo.15705180 (Chen, 2025).

Author contributions. HZX and BH conceived the central idea. QAC and HZX conducted most of the analyses and generated the Figures. QAC, BH and HZX wrote the main manuscript. DXW, CLL, ZYZ, HCJ contributed to the revision of the manuscript. HZX, ZYZ, HCJ, WS, TL, LW, SML and RJC conducted observations of the Mooring Array and participated in data analysis.

Competing interests. The contact author has declared that none of the authors has any competing interests.

Disclaimer. Publisher's note: Copernicus Publications remains neutral with regard to jurisdictional claims made in the text, published maps, institutional affiliations, or any other geographical representation in this paper. While Copernicus Publications makes every effort to include appropriate place names, the final responsibility lies with the authors. Also, please note that this paper has not received English language copy-editing. Views expressed in the text are those of the authors and do not necessarily reflect the views of the publisher.

Financial support. This research is supported by Hainan Provincial Natural Science Foundation of China (grant no. 423RC547), the National Natural Science Foundation of China (grant nos. 42376023, 42176033), the Natural Science Foundation of Guangdong Province (grant no. 2024A1515012218), the Innovational Fund for Scientific and Technological Personnel of Hainan Province (grant no. KJRC2023D39), the Southern Marine Science and Engineer-

ing Guangdong Laboratory (Zhuhai) (grant nos. SML2024SP009, SML2023SP240) and the innovation team of Deep Sea and Open Ocean Multi-Scale Dynamic Processes in the Southern Marine Science and Engineering Guangdong Laboratory (Zhuhai) (grant no. 311024005).

Review statement. This paper was edited by Sjoerd Groeskamp and reviewed by two anonymous referees.

References

- Alford, M. H.: Internal Swell Generation: The Spatial Distribution of Energy Flux from the Wind to Mixed Layer Near-Inertial Motions, J. Phys. Oceanogr., 31, 2359–2368, 2001.
- Alford, M. H.: Redistribution of energy available for ocean mixing by long-range propagation of internal waves, Nature, 423, 159–162, 2003.
- Alford, M. H.: Revisiting Near-Inertial Wind Work: Slab Models, Relative Stress, and Mixed Layer Deepening, J. Phys. Oceanogr., 50, 3141–3156, 2020.
- Alford, M. H., MacKinnon, J. A., Simmons, H. L., and Nash, J. D.: Near-Inertial Internal Gravity Waves in the Ocean, Annu. Rev. Mar. Sci., 8, 95–123, 2016.
- Barkan, R., Srinivasan, K., Yang, L., McWilliams, J. C., Gula, J., and Vic, C.: Oceanic Mesoscale Eddy Depletion Catalyzed by Internal Waves, Geophys. Res. Lett., 48, e2021GL094376, https://doi.org/10.1029/2021GL094376, 2021.
- Chen, Q.: Enhancement of near inertial waves by cyclonic eddy in the northwestern South China Sea during spring 2022, Zenodo [data set], https://doi.org/10.5281/zenodo.15705180, 2025.
- Chen, G., Hou, Y., and Chu, X.: Mesoscale eddies in the South China Sea: Mean properties, spatiotemporal variability, and impact on thermohaline structure, J. Geophys. Res., 116, C06018, https://doi.org/10.1029/2010JC006716, 2011.
- Chen, G., Xue, H., Wang, D., and Xie, Q.: Observed near-inertial kinetic energy in the northwestern South China Sea, J. Geophys. Res.-Oceans, 118, 4965–4977, 2013.
- Chen, S., Chen, D., and Xing, J.: A study on some basic features of inertial oscillations and near-inertial internal waves, Ocean Sci., 13, 829–836, https://doi.org/10.5194/os-13-829-2017, 2017.
- Chen, Z., Yu, F., Chen, Z., Wang, J., Nan, F., Ren, Q., Hu, Y., Cao, A., and Zheng, T.: Downward Propagation and Trapping of Near-Inertial Waves by a Westward-Moving Anticyclonic Eddy in the Subtropical Northwestern Pacific Ocean, J. Phys. Oceanogr., 53, 2105–2120, 2023.
- Chu, F., Si, Z., Yan, X., Liu, Z., Yu, J., and Pang, C.: Physical structure and evolution of a cyclonic eddy in the Northern South China sea, Deep-Sea Res. Pt. I, 189, 103876, https://doi.org/10.1016/j.dsr.2022.103876, 2022.
- Chu, X., Xue, H., Qi, Y., Chen, G., Mao, Q., Wang, D., and Chai, F.: An exceptional anticyclonic eddy in the South China Sea in 2010, J. Geophys. Res.-Oceans, 119, 881–897, 2014.
- Dasaro, E. A.: The Energy Flux from the Wind to near-Inertial Motions in the Surface Mixed Layer, J. Phys. Oceanogr., 15, 1043–1059, 1985.
- Esposito, G., Donnet, S., Berta, M., Shcherbina, A. Y., Freilich, M., Centurioni, L., D'Asaro, E. A., Farrar, J. T., Johnston, T. M. S.,

- Mahadevan, A., Özgökmen, T., Pascual, A., Poulain, P.-M., Ruiz, S., Tarry, D. R., and Griffa, A.: Inertial Oscillations and Frontal Processes in an Alboran Sea Jet: Effects on Divergence and Vertical Transport, J. Geophys. Res.-Oceans, 128, e2022JC019004, https://doi.org/10.1029/2022JC019004, 2023.
- Fan, L., Sun, H., Yang, Q., and Li, J.: Numerical investigation of interaction between anticyclonic eddy and semidiurnal internal tide in the northeastern South China Sea, Ocean Sci., 20, 241– 264, https://doi.org/10.5194/os-20-241-2024, 2024.
- Ferrari, R. and Wunsch, C.: Ocean Circulation Kinetic Energy: Reservoirs, Sources, and Sinks, Annu. Rev. Fluid Mech., 41, 253–282, 2009.
- Garrett, C.: What is the "near-inertial" band and why is it different from the rest of the internal wave spectrum?, J. Phys. Oceanogr., 31, 962–971, 2001.
- Guo, M., Chen, R., Xu, H., and Vetter, P. A.: Dynamical features of near-inertial motions in global ocean based on the GDP dataset from 2000 to 019, Acta Oceanolog. Sin., 40, 126–134, 2021.
- He, Q., Zhan, H., Cai, S., He, Y., Huang, G., and Zhan, W.: A New Assessment of Mesoscale Eddies in the South China Sea: Surface Features, Three-Dimensional Structures, and Thermohaline Transports, J. Geophys. Res.-Oceans, 123, 4906–4929, 2018.
- Hersbach, H., Bell, B., Berrisford, P., Biavati, G., Horányi, A., Muñoz Sabater, J., Nicolas, J., Peubey, C., Radu, R., Rozum, I., Schepers, D., Simmons, A., Soci, C., Dee, D., Thépaut, J.-N.: ERA5 hourly data on single levels from 1940 to present, Copernicus Climate Change Service (C3S) Climate Data Store (CDS) [data set], https://doi.org/10.24381/cds.adbb2d47, 2023.
- Huang, X., Wang, Z., Zhang, Z., Yang, Y., Zhou, C., Yang, Q., Zhao, W., and Tian, J.: Role of Mesoscale Eddies in Modulating the Semidiurnal Internal Tide: Observation Results in the Northern South China Sea, J. Phys. Oceanogr., 48, 1749–1770, 2018.
- Jing, Z., Wu, L., and Ma, X.: Energy Exchange between the Mesoscale Oceanic Eddies and Wind-Forced Near-Inertial Oscillations, J. Phys. Oceanogr., 47, 721–733, 2017.
- Jing, Z., Chang, P., DiMarco, S. F., and Wu, L.: Observed Energy Exchange between Low-Frequency Flows and Internal Waves in the Gulf of Mexico, J. Phys. Oceanogr., 48, 995–1008, 2018.
- Klein, P., Hua, B. L., and Carton, X.: Emergence of cyclonic structures due to the interaction between near-inertial oscillations and mesoscale eddies, Q. J. Roy. Meteorol. Soc., 129, 2513–2525, 2003.
- Kunze, E.: Near-Inertial Wave Propagation In Geostrophic Shear, J. Phys. Oceanogr., 15, 544–565, 1985.
- Li, Q., Chen, Z., Guan, S., Yang, H., Jing, Z., Liu, Y., Sun, B., and Wu, L.: Enhanced Near-Inertial Waves and Turbulent Diapycnal Mixing Observed in a Cold- and Warm-Core Eddy in the Kuroshio Extension Region, J. Phys. Oceanogr., 52, 1849–1866, 2022.
- Lin, P., Fang, W., Chen, Y., and Tang, X.: Temporal and spatial variation characteristics on eddies in the South China Sea I. Statistical analyses, Acta Oceanolog. Sin., 29, 14–22, 2007.
- Liu, G., Chen, Z., Lu, H., Liu, Z., Zhang, Q., He, Q., He, Y., Xu, J., Gong, Y., and Cai, S.: Energy Transfer Between Mesoscale Eddies and Near-Inertial Waves From Surface Drifter Observations, Geophys. Res. Lett., 50, e2023GL10472, https://doi.org/10.1029/2023GL104729, 2023.

- Liu, Y., Jing, Z., and Wu, L.: Wind Power on Oceanic Near-Inertial Oscillations in the Global Ocean Estimated From Surface Drifters, Geophys. Res. Lett., 46, 2647–2653, 2019.
- Nan, F., Xue, H., Xiu, P., Chai, F., Shi, M., and Guo, P.: Oceanic eddy formation and propagation southwest of Taiwan, J. Geophys. Res.-Oceans, 116, C12045, https://doi.org/10.1029/2011JC007386, 2011.
- Oey, L. Y., Ezer, T., Wang, D. P., Fan, S. J., and Yin, X. Q.: Loop Current warming by Hurricane Wilma, Geophys. Res. Lett., 33, L08613, https://doi.org/10.1029/2006GL025873, 2006.
- Ouyang, Z., Liu, Z., Sun, Y., Yang, B., and Hou, Y.: Observation of Near Inertial Waves Induced by Typhoon Mitag (2019) on the Southwestern East China Sea Continental Slope, Journal of Marine Science and Engineering, 10, 202, https://doi.org/10.3390/jmse10020202, 2022.
- Provenzale, A.: Transport by Coherent Barotropic Vortices, Annu. Rev. Fluid Mech., 31, 55–93, 1999.
- Thomas, J. and Daniel, D.: Turbulent exchanges between near-inertial waves and balanced flows, J. Fluid Mech., 902, A7-1–A7-27, https://doi.org/10.1017/jfm.2020.510, 2020.
- Thomas, L. N.: On the modifications of near-inertial waves at fronts: implications for energy transfer across scales, Ocean Dynam., 67, 1335–1350, 2017.
- Voet, G., Waterhouse, A. F., Savage, A., Kunze, E., Mackinnon, J. A., Alford, M. H., Colosi, J. A., Simmons, H. L., Klenz, T., and Kelly, S. M.: Near-inertial energy variability in a strong mesoscale eddy field in the Iceland basin, Oceanography, 37, 34–37, https://doi.org/10.5670/oceanog.2024.302, 2024.
- Wang, G., Su, J., and Chu, P. C.: Mesoscale eddies in the South China Sea observed with altimeter data, Geophys. Res. Lett., 30, 2121, https://doi.org/10.1029/2003GL018532, 2003.
- Wang, G., Chen, D., and Su, J.: Winter Eddy Genesis in the Eastern South China Sea due to Orographic Wind Jets, J. Phys. Oceanogr., 38, 726–732, 2008.
- Wang, X., Du, Y., Zhang, Y., Wang, T., Wang, M., and Jing, Z.: Subsurface Anticyclonic Eddy Transited from Kuroshio Shedding Eddy in the Northern South China Sea, J. Phys. Oceanogr., 53, 841–861, 2023.
- Weller, R. A.: The Relation of Near-Inertial Motions Observed in the Mixed layer During the JASIN (1978) Experiment to the Local Wind Stress and to the Quasi-Geostrophic Flow Field, J. Phys. Oceanogr., 12, 1122–1136, 1982.
- Xiu, P., Chai, F., Shi, L., Xue, H., and Chao, Y.: A census of eddy activities in the South China Sea during 1993–2007, J. Geophys. Res.-Oceans, 115, C03012, https://doi.org/10.1029/2009JC005657, 2010.
- Xu, H., Zhang, Z., Vetter, P. A., Xie, Q., Long, T., and Hong, B.: Impact of Anticyclonic Eddy on Nonlinear Wave–Wave Interaction in the Southern South China Sea During Late Summer 2020, Geophys. Res. Lett., 49, e2021GL096892, https://doi.org/10.1029/2021GL096892, 2022a.
- Xu, X., Zhao, W., Huang, X., Hu, Q., Guan, S., Zhou, C., and Tian, J.: Observed Near-Inertial Waves Trapped in a Propagating Anticyclonic Eddy, J. Phys. Oceanogr., 52, 2029–2047, 2022b.
- Yu, X., Naveira Garabato, A. C., Vic, C., Gula, J., Savage, A. C., Wang, J., Waterhouse, A. F., and MacKinnon, J. A.: Observed Equatorward Propagation and Chimney Effect of Near-Inertial Waves in the Midlatitude Ocean, Geophys. Res. Lett., 49, e2022GL098522, https://doi.org/10.1029/2022GL098522, 2022.

- Yuan, S., Yan, X., Zhang, L., Pang, C., and Hu, D.: Observation of Near Inertial Waves Induced by Typhoon Lan in the Northwestern Pacific: Characteristics, Energy Fluxes and Impact on Diapycnal Mixing, Journal of Geophysical Research: Oceans, 129, 12, https://doi.org/10.1029/2023JC020187, 2024.
- Zhai, X., Johnson, H. L., and Marshall, D. P.: Significant sink of ocean-eddy energy near western boundaries, Nat. Geosci., 3, 608–612, 2010.
- Zhang, W. Z., Xue, H., Chai, F., and Ni, Q.: Dynamical processes within an anticyclonic eddy revealed from Argo floats, Geophys. Res. Lett., 42, 2342–2350, 2015.
- Zhang, Z., Tian, J., Qiu, B., Zhao, W., Chang, P., Wu, D., and Wan, X.: Observed 3D Structure, Generation, and Dissipation of Oceanic Mesoscale Eddies in the South China Sea, Sci. Rep., 6, 24349, https://doi.org/10.1038/srep24349, 2016.
- Zhang, Z., Liu, Z., Richards, K., Shang, G., Zhao, W., Tian, J., Huang, X., and Zhou, C.: Elevated Diapycnal Mixing by a Subthermocline Eddy in the Western Equatorial Pacific, Geophys. Res. Lett., 46, 2628–2636, 2019.

- Zhang, Z., Liu, Y., Qiu, B., Luo, Y., Cai, W., Yuan, Q., Liu, Y., Zhang, H., Liu, H., Miao, M., Zhang, J., Zhao, W., and Tian, J.: Submesoscale inverse energy cascade enhances Southern Ocean eddy heat transport, Nat. Commun., 14, 1335, https://doi.org/10.1038/s41467-023-36991-2, 2023.
- Zhao, B., Xu, Z., Li, Q., Min, W., Wang, Y., and Yin, B.: The characteristics of spontaneous near-inertial wave generation from an anticyclonic mesoscale eddy, J. Oceanol. Limnol., 40, 413–427, 2021
- Zhao, B., Liu, Z., Xu, Z., Yin, B., and Zheng, Q.: Spontaneous near-inertial wave generation from mesoscale eddy: Nonlinear forcing mechanism, Phys. Fluids, 35, 076609, https://doi.org/10.1063/5.0156176, 2023.